

PREPARED FOR SUBMISSION TO JHEP

DCPT/21/54
DESY 21-135
IPPP/21/27
MCNET-21-14
SAGEX-21-29

Unbiased Elimination of Negative Weights in Monte Carlo Samples

Jeppe R. Andersen^a and Andreas Maier^b

^a*Institute for Particle Physics Phenomenology, University of Durham, Durham, DH1 3LE, UK*

^b*Deutsches Elektronen-Synchrotron DESY, Platanenallee 6, 15738 Zeuthen, Germany*

ABSTRACT: We propose a novel method for the elimination of negative Monte Carlo event weights. The method is process-agnostic, independent of any analysis, and preserves all physical observables. We demonstrate the overall performance and systematic improvement with increasing event sample size, based on predictions for the production of a W boson with two jets calculated at next-to-leading order perturbation theory.

Contents

1	Introduction	1
2	Cell Resampling	2
2.1	Distances in Phase Space	3
2.1.1	Definition of the Distance Function	4
2.1.2	Alternative Norms	5
2.1.3	Example for an Event Distance	7
2.2	Nearest-Neighbour Search and Locality-Sensitive Hashing	7
2.3	Relation to Positive Resampling	11
3	Cell Resampling for the Production of a W Boson with two Jets	11
4	Conclusions	15

1 Introduction

The LHC physics programme has entered an era of precision measurements. Such measurements demand equally precise theory predictions. To match this requirement, it is most often necessary to include at least next-to-leading order (NLO) perturbative corrections. For a number of processes, even higher fixed-order corrections, i.e. NNLO and NNNLO, have to be taken into account. In order to consistently combine virtual corrections, usually computed in $d = 4 - 2\epsilon$ dimensions, and real corrections, obtained via numerical integration over four-dimensional momenta, one introduces subtraction terms which render each component finite, see for example [1, 2].

Since one is usually interested in distributions, additional effects from parton showers and hadronisation have to be accounted for. Methods such as MC@NLO [3] and POWHEG [4] can be employed for matching parton showers and NLO fixed-order predictions. Depending on the phase-space region of interest, further resummation may be required. Examples include transverse momentum [5] and high-energy resummation [6, 7]. High-accuracy predictions for multi-jet observables are then obtained by merging exclusive event samples using e.g. the MEPS@NLO [8] or UNLOPS [9, 10] approaches. Finally, the detector response to the generated events is simulated [11].

Thanks to continuous improvements, modern general purpose event generators [12–15] render the inclusion of many of these corrections feasible for a large range of scattering processes. However, the improved accuracy comes at a significant cost in computing time. What is more, each of the individual calculational steps outlined above also increases the cost of all subsequent steps. The reason for this is that typically a number of negative-weight counterevents are generated, for instance for unitarisation or in order to prevent

double counting. This implies that a much larger number of events has to be processed to reach the same statistical significance as for the case of purely positive-weight event samples. This problem is particularly pronounced in the final detector simulation step, which can take hours of CPU time for each event.

Consequently, there have been a number of recent efforts to ameliorate this problem. One avenue that is being explored is to reduce the fraction of negative-weight events that are produced during the generation [16–19]. An alternative approach is to remove such events altogether from the generated samples, while taking care that observables are not affected [20–22]. The algorithm proposed in [20] has been shown to be very effective in a highly non-trivial example. However, there are two caveats. First, the algorithm requires the choice of an auxiliary distribution, despite being process-agnostic in nature. Second, while the algorithm has been shown to produce sound results in practice, a proof of the correctness has only been given for a specific set of observables related to the chosen distribution.

In the following, we present a novel method, dubbed *cell resampling*, which eliminates negative event weights locally in phase space, is independent of the underlying process, and preserves all physical observables. We describe our method in section 2, and apply it to a calculation of W boson production with two jets at next-to-leading order in section 3. We conclude with a summary and an outlook in section 4.

2 Cell Resampling

The integrated physical cross section over any slice of phase space has to be non-negative. This well-known fact is the key observation at the core of the cell resampling method.

Let us consider a Monte Carlo event sample with mixed positive and negative event weights, together with an analysis we want to perform. We now focus on a single event with negative weight, our *seed*, and consider a small solid sphere in phase space that is centred around said event and contains no other events. We call this sphere a *cell*. We then gradually increase the radius of the cell until the sum over all weights of events contained inside the cell is non-negative.

The key point is that with sufficiently many generated events, this cell can be made arbitrarily small. In particular, it can be made much smaller than the resolution of the analysis. At this point, we may freely redistribute the weights of the events within the cell without affecting the analysis results. In particular, we replace all event weights by their absolute value and rescale them such that the sum of weights is preserved. That is, we perform the replacement

$$w_i \rightarrow \frac{\sum_{j \in \mathcal{C}} w_j}{\sum_{j \in \mathcal{C}} |w_j|} |w_i| \quad (2.1)$$

for all weights w_i of events i inside the cell \mathcal{C} . This accomplishes the original intent behind the generation of negative-weight counter-events: any overestimation of the cross section from positive-weight events is cancelled *locally* in phase space.

After applying the above steps successively to each negative-weight event we are left with a physically equivalent sample of all positive-weight events. Note that the method is

completely agnostic to any details of the event generation, including the underlying process, and does not refer to any properties of the analysis. The only prerequisite is sufficiently high statistics, so that single cells are not resolved by the analysis.

In practice, it may not be feasible to generate and resample enough events to reach this goal. A particular concern is posed by cells containing events in different bins. Small enough cells close to bin boundaries can even turn out to be beneficial by smoothing out statistical jitter due to bin migration. However, as cells grow larger, the resampling will start to smear out characteristic features of distributions, such as resonance peaks.

To prevent this smearing, we can impose an upper limit on the cell sizes, at the cost of some cells not containing sufficient positive weight events to cancel the contribution from events with negative weight. This implies that we no longer eliminate all of the negative event weights. Still, since at least part of the negative seed event weight is absorbed by surrounding events, a subsequent unweighting will reduce the fraction of negative-weight events compared to the original sample. The size of cells with negative accumulated weight is related to the extent in phase space of counter-terms, and as such is related to the usual problems with bin-to-bin migration in higher-order calculations.

For the sake of a streamlined presentation, we will allow cells to grow arbitrarily large for the remainder of this section. We will come back to the discussion of a cell size limit when analysing the practical performance of our method in section 3.

2.1 Distances in Phase Space

A central ingredient in cell resampling is the definition of a universal distance function in phase space. The aim here is to reflect the experimental sensitivity: events with similar detector responses should be close to each other according to the distance measure. However, at the same time the distance function should be independent of any specific analysis details.

On the one hand, two events with vastly different sets of outgoing particles with large differences in particle momenta should have a large distance according to the chosen metric. On the other hand, two events containing the same particles with only slightly different momenta should be very close. Adding further soft particles to one of the events should only change the distance by a small amount. Specifically, adding particles with vanishing four-momentum should not affect distances at all.

We also require infrared safety, i.e. the distance function has to be insensitive to collinear splittings or soft radiation inside jets. At first glance, this seems to introduce an unwanted dependence on analysis parameters, namely on the jet definition. However, since already the event generation depends on this definition, referring to it does not limit the generality of our approach. The metric is sensitive to the event sample in question, but not to the analysis.

Keeping these requirements in mind, we now define a concrete distance function, which we use in the following. Note that our choice is by no means unique and we do not claim that our definition is optimal. A particularly promising alternative is the “energy mover’s distance” introduced in [23] and generalised to include flavour information in [24]. We leave a detailed comparison between different distance functions to future work.

2.1.1 Definition of the Distance Function

As a first step, we cluster the partons in each event into jets. We then group outgoing particles into sets according to their types, i.e. according to all discrete observable properties such as flavour and charge. Particles which only differ by their four-momenta (including possible differences in their invariant masses) end up inside the same set. For the time being, we do not differentiate between polarisations or various types of jets, but it is straightforward to add such distinctions.

The distance d between an event e with T particle type sets $\mathcal{S} = \{s_1, s_2, \dots, s_T\}$ and an event e' with sets $\mathcal{S}' = \{s'_1, s'_2, \dots, s'_T\}$ is then given by the sum of the distances between matching sets, i.e.

$$d(e, e') = \sum_{t=1}^T d(s_t, s'_t), \quad (2.2)$$

where s_t, s'_t contain all particles of type t that occur in the respective event. If there are no particles of type t in a given event, then the corresponding set is empty. This ensures that all events in the sample have the same number of particle type sets.

Next, we have to define the distance between a set s_t , containing P particles of type t with four-momenta p_1, \dots, p_P and a set s'_t with Q particles of the same type with four-momenta q_1, \dots, q_Q . Without loss of generality we can assume $Q \leq P$. To facilitate the following steps we first add $P - Q$ particles with vanishing momenta to the set Q , i.e. we define the momenta

$$q_{Q+1} = \dots = q_P = 0. \quad (2.3)$$

Naturally, the distance between s_t and s'_t must not depend on the labeling of the momenta. We therefore consider all permutations of the momenta q_1, \dots, q_P and sum the pairwise distances to the momenta p_1, \dots, p_P for each permutation. The minimum defines the distance between s and s' :

$$d(s_t, s'_t) = \min_{\sigma \in S_P} \sum_{i=1}^P d(p_i, q_{\sigma(i)}). \quad (2.4)$$

Here, S_P denotes the symmetric group, i.e. the group of all permutations of P elements.

While this distance function is obviously invariant under relabelling and when adding vanishing momenta, its calculation quickly becomes prohibitively expensive when the number of momenta P in the sets grows large. More precisely, the computational cost scales as $\mathcal{O}(P!) = \mathcal{O}\left(P^{P+\frac{1}{2}}\right)$. For events obtained through fixed-order calculations, P is typically small enough and the poor scaling is not a concern. However, after parton showering, large values of $P \approx 10$ can be reached. In such cases, we use an alternative distance function \tilde{d} which is easier to compute. We first define a unique labelling by ordering the momenta according to their norm

$$\|p_i\| \equiv d(p_i, 0), \quad \|q_i\| \equiv d(q_i, 0). \quad (2.5)$$

We then search for the nearest neighbour of p_1 in Q , i.e. the momentum $q_{\text{NN}(1)} \in Q$ that minimises the distance to p_1 :

$$d(p_1, q_{\text{NN}(1)}) \leq d(p_1, q_i) \quad \forall q_i \in s'_t. \quad (2.6)$$

In the next step, we find the nearest neighbour $q_{\text{NN}(2)}$ of p_2 , *excluding* the momentum $q_{\text{NN}(1)}$ and add $d(p_2, q_{\text{NN}(2)})$ to the total distance. We iteratively define further exclusive nearest neighbours $\text{NN}(j)$ by removing previous ones,

$$s'_{t,\bar{j}} = s'_t \setminus \{q_{\text{NN}(1)}, \dots, q_{\text{NN}(j-1)}\}, \quad (2.7)$$

and finding the element $q_{\text{NN}(j)}$ such that

$$d(p_j, q_{\text{NN}(j)}) \leq d(p_j, q_i) \quad \forall q_i \in s'_{t,\bar{j}}. \quad (2.8)$$

Finally, we add up all these distances. To arrive at a symmetric distance function, we compare to the total distance obtained by exchanging s_t and s'_t . The smaller of the two distances defines $\tilde{d}(s_t, s'_t)$:

$$\tilde{d}(s_t, s'_t) = \min \left(\sum_{i=1}^P d(p_i, q_{\text{NN}(i)}), \sum_{i=1}^P d(q_i, p_{\text{NN}(i)}) \right). \quad (2.9)$$

Since this minimises over only two out of all possible sets of pairings between momenta p_i and q_j , $\tilde{d}(s_t, s'_t)$ scales as $\mathcal{O}(P^2)$ instead of $\mathcal{O}(P^{P+\frac{1}{2}})$. For the same reason, it is bounded from below by $d(s_t, s'_t)$. However, for nearby events we expect that the exclusive nearest neighbours $\text{NN}(i)$ defined above coincide with the *actual* nearest neighbours. In this case the distance functions \tilde{d} and d will yield the same result. Let us finally remark that \tilde{d} also remains unchanged when adding vanishing momenta to the sets s_t and s'_t .

The last missing ingredient is the distance $d(p, q)$ between two momenta p and q . One can in principle choose different distance functions for different particles types (e.g. to include only transverse momentum for neutrinos), but for simplicity we will in this study apply the same distance for all types. Note that the Minkowski distance $\sqrt{(p-q)_\mu (p-q)^\mu}$ is *not* a suitable distance. Such a distance would be insensitive to lightlike differences between momenta, which does not match the reality of experimental measurements. Since, for a given particle mass, only three momentum components are independent, our distance measure is based on the difference in *spatial* momentum. Anticipating the fact that experimental measurements are more sensitive to the perpendicular momentum components we further add a rescaled difference in transverse momenta:

$$d(p, q) = \sqrt{\sum_{i=1}^3 (p_i - q_i)^2 + \tau^2 (p_\perp - q_\perp)^2}. \quad (2.10)$$

τ is a tunable parameter. Further terms can be added, e.g. in order to introduce sensitivity to different jet masses.

2.1.2 Alternative Norms

The choice of a momentum distance function is not unique and one could alternatively consider other coordinate systems, such as light-cone coordinates, or general p-norms

$$d_p(p, q) = \left(\sum_{i=1}^3 (p_i - q_i)^p \right)^{\frac{1}{p}}. \quad (2.11)$$

One interesting possibility yet to be explored is to take inspiration from jet distance measures and employ a distance in rapidity or azimuthal angle, which has to be combined with a transverse momentum distance in a meaningful way. We leave such explorations to further study.

It is, in any case, crucial to not violate the triangle inequality

$$d(p, q_1 + q_2) \leq d(p, q_1) + d(p, q_2). \quad (2.12)$$

To illustrate this point, let us consider the *square* of the spatial norm

$$d^2(p, q) = \sum_{i=1}^3 (p_i - q_i)^2, \quad (2.13)$$

a set s with one particle momentum p_1 , and a set s' with one particle momentum q_1 . For simplicity, let us assume one-dimensional momenta with $p_1 = 2$ and $q_1 = -2$ in arbitrary units. Since there is only one possible pairing of momenta, the event distance is $d_2(s, s') = d(p_1, q_1) = 4$ using the spatial $p = 2$ norm and $d^2(s, s') = d^2(p_1, q_1) = 16$ when using the square.

We now add one particle with vanishing momentum to each s and s' , reminding ourselves that this change is not experimentally detectable and therefore must not affect the distance between the sets. This scenario is shown in figure 1. According to equation (2.4) the set distance is now given by

$$d(s, s') = \min \left[d(p_1, q_1) + d(p_2, q_2), d(p_1, q_2) + d(p_2, q_1) \right], \quad p_2 = q_2 = 0, \quad (2.14)$$

with $d(p_2, q_2) = 0$ for either choice. For the spatial norm both permutations yield the same result and $d_2(s, s') = 4$ as before. However, if we use the square d^2 instead, we find that the triangle inequality is violated and $d^2(s, s') = 8$ instead of 16.

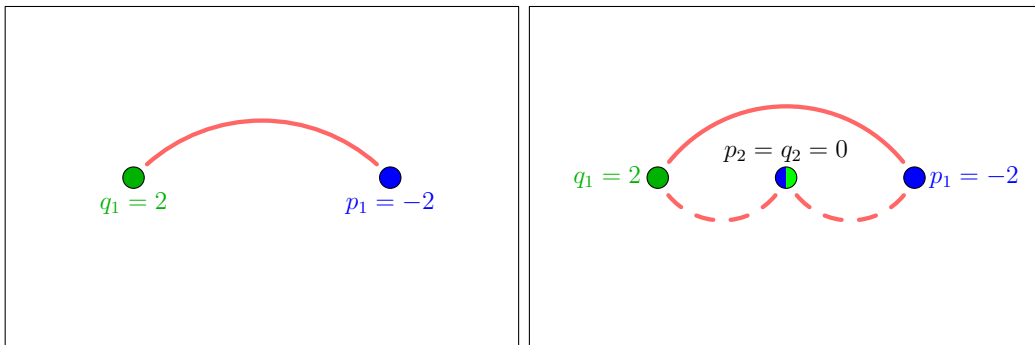


Figure 1: Distances between two sets s, s' , each of which contains one particle (left panel) or two particles (right panel). Blue dots represent particles in set s , green dots stand for particles in set s' . The possible pairings used in the distance calculation are indicated by lines. The square norm d^2 erroneously results in a shorter distance for the pairing indicated by the dashed line.

2.1.3 Example for an Event Distance

To illustrate one possible distance measure, let us consider a simple yet non-trivial example, where we calculate the distance between two events e and e' . e has two outgoing photons and a jet, and e' two photons and no jets. The distance between the two events is therefore

$$d(e, e') = d(s_\gamma, s'_\gamma) + d(s_j, s'_j). \quad (2.15)$$

The jet set s_j for the event e contains a single jet with momentum p_j , whereas the corresponding set s'_j for e' is empty. Likewise, s_γ contains the photons in e with momenta p_1, p_2 and s'_γ the photons in e' with momenta p'_1, p'_2 . The distance between these two sets is

$$d(s_\gamma, s'_\gamma) = \min \left[d(p_1, p'_1) + d(p_2, p'_2), d(p_1, p'_2) + d(p_2, p'_1) \right], \quad (2.16)$$

where $d(p, q) = \sqrt{\sum_{i=1}^3 (p_i - q_i)^2 + \tau^2 (p_\perp - q_\perp)^2}$ is the distance introduced in equation (2.10).

To calculate the distance $d(s_j, s'_j)$ between the jet sets, we first add an auxiliary “jet” with vanishing momentum $p'_j = 0$ to s'_j , so that both sets each contain a single jet. The set distance is then

$$d(s_j, s'_j) = d(p_j, p'_j) = \sqrt{\sum_{i=1}^3 p_{ji}^2 + \tau^2 p_{j\perp}^2}, \quad (2.17)$$

where p_j denotes the momentum of the physical jet.

2.2 Nearest-Neighbour Search and Locality-Sensitive Hashing

A very appealing feature of cell resampling is that the cell radii automatically become smaller with increasing number of events. Anticipating the discussion of the practical application with the distance measure in section 3, we indeed find a significant reduction in cell size, as shown in figure 2. Due to large fluctuations in the weights of the cell seeds, and correspondingly in the cell sizes, we consider the median of the cell radii instead of the arithmetic mean.

From this point of view, cell resampling should be applied to event samples that are as large as possible. However, the main motivation behind the resampling is to reduce the computational cost of later steps. This implies that the CPU time needed for resampling should be much smaller. On the one side, various event generation steps are usually performed on an event-by-event basis, and the asymptotic generation time scales linearly with the number n of events. On the other side, the number of negative-weight events and therefore the number of cells are also proportional to n . To achieve the same asymptotic $\mathcal{O}(n)$ runtime scaling, the time to construct a single cell has to be constant, i.e. independent of the sample size. However, while obviously asymptotically inferior, overall $\mathcal{O}(n \log^k n)$ scaling for some integer k will presumably be sufficient for real-world sample sizes.

To reiterate, a cell is constructed as follows. We choose a seed, i.e. one of the remaining negative-weight events. As long as the sum of weights inside the cell is negative, we subsequently find the closest event to the seed outside the cell according to our distance function and add it to the cell. Finally, we reweight all events inside the cell.

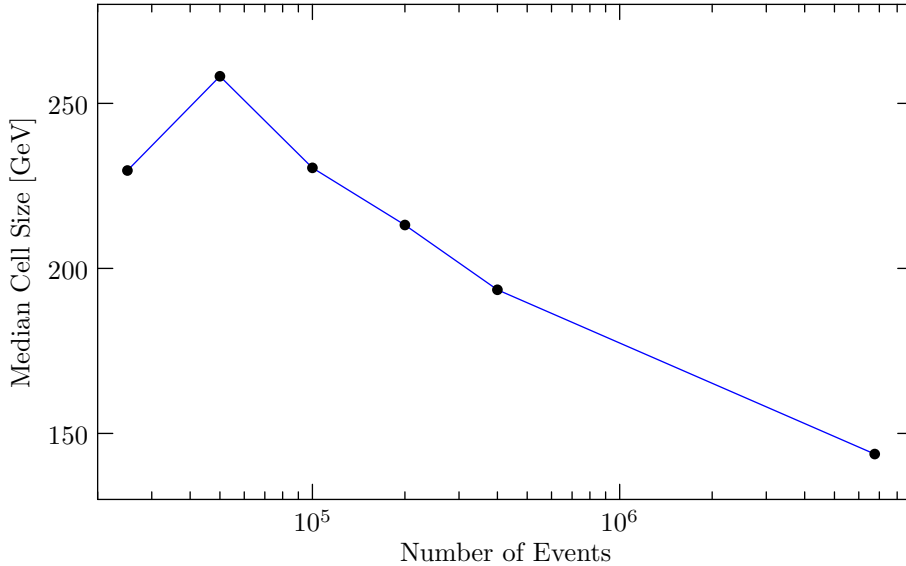


Figure 2: Median cell radius as a function of sample size according to the distance measure defined in section 2.1.1 with $\tau = 0$. See section 3 for details on the event generation.

The selection of a negative-weight event can be achieved in constant time with the help of a pregenerated array containing these events, which can be created in $\mathcal{O}(n)$ steps. If we want to construct cells in a specific order, an additional $\mathcal{O}(n \log n)$ sorting step is required. Indeed, the distribution of cell sizes can be quite sensitive to the construction order, but it is not obvious which ordering is best in this regard. By default, we first choose the events with the most negative weights as seeds. Empirically, we find that this choice leads to faster cell construction than a random ordering.

The biggest challenge is to find nearby events in constant or, at worst, logarithmic time. A naive nearest-neighbour search requires $\mathcal{O}(n)$ operations for each cell, leading to an overall $\mathcal{O}(n^2)$ scaling. Nearest-neighbour search is a well-studied problem in computer science. In modern particle physics, one of the most prominent applications is jet clustering [25]. However, jet clustering requires searches in two dimensions and the algorithms used there are not suited for the present high-dimensional problem. For approximate searches in high-dimensional spaces, *locality-sensitive hashing* (LSH) [26, 27] has been found to be highly efficient. In the following we give a short outline while describing one way in which LSH can be used for finding events that are close to a given cell.

First, we relax the condition that cells have to be kept spherical by subsequently adding nearest neighbours. We will contend ourselves with cells that are small in each phase-space direction and, most importantly, shrink with increasing statistics. This can be achieved by an approximate nearest-neighbour search.

In order to being able to apply standard techniques, we map the events onto points in a high-dimensional Euclidean space. A crucial observation is that this map does not have to preserve distances, neither in the absolute nor in the relative sense. It is sufficient that events that are nearby in phase space are mapped onto points that are nearby in Euclidean

space with high probability. To this end, we recall that, in each event e , we group particles into sets $s_{e,t}$ according to their type t . To each of these sets, we now add particles with vanishing four-momentum until for each particle type all sets in all events have the same number of elements,¹ i.e.

$$|s_{e,t}| = |s_{e',t}| \quad \text{for all events } e, e' \text{ and types } t. \quad (2.18)$$

We then interpret each set $s_{e,t}$ as a tuple $\tau_{e,t} = (p_{e,t,1}, \dots, p_{e,t,P_t})$ of P_t four-momenta, which we sort lexicographically according to the momentum components. Finally, for the event e the coordinates of the resulting point V_e in Euclidean space correspond to the spatial momentum components in order. The first three components $i = 1, 2, 3$ are obtained from the first spatial momentum in the tuple for the first particle type, i.e. $(V_e)_i = (p_{e,1,1})_i$. The next three components correspond to the second momentum in the tuple for the first particle type, and after reaching the last momentum in a tuple we proceed to the tuple for the next particle type. The total dimension of the Euclidean space is therefore

$$D = 3 \sum_{t=1}^T |s_{e,t}|, \quad (2.19)$$

which is independent of the chosen event e . Events e and e' which are nearby in phase space will most likely have a similar number of outgoing particles of each type with similar momenta. Therefore, the coordinates of V_e and $V_{e'}$ will be similar and the points will be close to each other.

We have now recast the problem to finding approximate nearest neighbours between the points V_e in a D -dimensional Euclidean space. To facilitate this task, we consider *random projections* onto lower dimensional sub spaces. This is a well-established technique motivated by the Johnson-Lindenstrauss Lemma [28], which states that it is always possible to find projections that nearly preserve the distances between the points. Specifically, we define projections Π_h onto hyperplanes $h = 1, \dots, H$, each fixed by a randomly chosen unit normal vector as discussed in [29, 30]. H should be chosen in such a way that it grows logarithmically with the number of points, i.e. the number of events. We then perform a second projection onto the x axis, i.e. we take the first coordinate of each projected vector:

$$V_e \mapsto c_{e,h} = (\Pi_h V_e)_1. \quad (2.20)$$

For each $h = 1, \dots, H$, we sort the coordinates $c_{e,h}$ obtained from all events e in the sample and divide them into *buckets* of size B . B may increase at worst logarithmically with the number of events, otherwise the described algorithm for cell creation would no longer fulfill our time complexity constraint, as shown later. Note that events e, e' with nearby coordinates $c_{e,h}, c_{e',h}$ will be inside the same bucket with high probability.

This effectively defines H *hash functions* f_h , each of which maps a given event onto a single integer number, namely the index of the bucket associated with the coordinate $c_{e,h}$:

$$f_h : \quad e \mapsto \text{bucket}[c_{e,h}] = \text{bucket}[(\Pi_h V_e)_1]. \quad (2.21)$$

¹Sets corresponding to different particle types may still have different cardinalities.

These hash functions are *locality sensitive*. Nearby events are likely to be mapped onto the same number.

We use the hash functions to create H *hash tables*, where we store the values of $f_h(e)$ for all events e . When creating a cell, we look up the hashed values $f_h(e)$ for the seed event e . We then consider all events that lie in the same bucket as e in one of the H projected coordinates, i.e. at most HB events. In practice, the number will be much lower, as nearby events will share more than one bucket with e . Starting from the events sharing the most buckets with e , we identify nearest neighbour candidates.² We select candidates with weights w_i , until we fulfil

$$\sum_i w_i \geq -aw_e, \quad (2.22)$$

where w_e is the (negative) seed weight and a an arbitrary constant with $a \geq 1$. In our implementation, we choose $a = 2$.

For each of the nearest neighbour candidate, we then compute the actual distance to the seed e using the metric defined in section 2.1. We proceed to add nearest neighbours according to the actual distance to the cell, as we did when using naive nearest-neighbour search, until the sum of weights inside the cell is no longer negative.

Let us now analyse the asymptotic time complexity of the LSH-based algorithm. To create the hash table, we have to compute H projected coordinates for each of the n events, where $H = \mathcal{O}(\log n)$. Once the H hyperplanes are fixed, each coordinate can be computed independently in constant time. In total we compute $\mathcal{O}(Hn) = \mathcal{O}(n \log n)$ coordinates. For each h , we have to sort the coordinates of n events, which gives a time complexity of $\mathcal{O}(Hn \log n) = \mathcal{O}(n \log^2 n)$. The partitioning into buckets is again linear in the number of events, and therefore asymptotically negligible compared to the sorting.

Looking up the values of the hash functions for a single seed event requires $\mathcal{O}(H) = \mathcal{O}(\log n)$ operations. To select the candidates we have to probe all events in H buckets of size B , with time complexity $\mathcal{O}(HB) = \mathcal{O}(\log^2 n)$. Since the number of events needed to compensate the seed weight does not increase with n , only a constant number of distance functions have to be calculated after selecting candidates. In total, the number of cells grows linearly with n and the creation of each cell requires $\mathcal{O}(\log^2 n)$ constant-time steps, which results in an overall time complexity of $\mathcal{O}(n \log^2 n)$.

Finally, we consider the practical performance of our implementation for various sample sizes. Figure 3 compares the median cell size, measured by the largest distance between the seed and any other event inside the cell, and scaling of the computing time to the naive linear nearest-neighbour search. Heuristically, we have chosen $H = 15 \log n$ hash functions and a fixed bucket size of $B = 1000$. We find that the required computing time indeed scales much better with increased sample size. However, the cell size does not seem to decrease significantly with larger statistics. We conclude that further improvements are needed to render the LSH-based approach competitive compared to the linear nearest-neighbour search.

²In principle, one could consider all events sharing buckets with e without violating the complexity constraints. However, in practice we only need a small fraction of these events to create the cell.

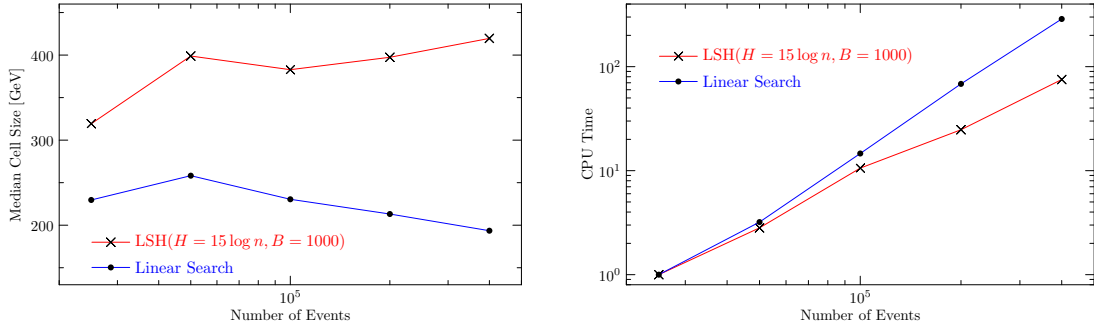


Figure 3: Comparison between linear nearest-neighbour search and the LSH-based approach with $H = 15 \log n$ hash functions and buckets containing $B = 1000$ events. The left panel shows the median cell size as a function of the number of input events. The right panel illustrates the scaling of the computing time with the sample size. The respective timings are normalised to the first data point in order to facilitate comparison and eliminate constant factors resulting from differences in the implementation.

2.3 Relation to Positive Resampling

Let us comment on the relation between the current approach and the positive resampler suggested in [20]. There, events are collected in histogram bins and positive resampling, i.e. replacing event weights by rescaled absolute values, is performed on each bin separately.

There is a clear parallel to the LSH-based method presented in section 2.2. Where the LSH includes random projections of events onto coordinates, positive resampling projects events onto one or more observables defined by the chosen histogram, such as particle transverse momenta. The histogram bins then correspond to the buckets in the locality-sensitive hash tables. Following the same philosophy behind the random projection method, we expect events in the same histogram bins to be also close in other phase-space directions with high probability.

Positive resampling as presented in [20] is therefore similar to cell resampling with LSH-based nearest-neighbour search with a small number of $H \leq 3$ hash functions. An important difference is the definition of a cell. The equivalent for the positive resampler would be an entire bin, i.e. a complete hash bucket. For this reason, it is difficult to perform a rigorous direct comparison between the two approaches. However, we can get an idea by comparing cell resampling with linear nearest-neighbour search and LSH-based search with small H . In figure 4 we compare the median cell sizes obtained in both approaches for different sample sizes. We have increased the bucket size to $B = 20000$ to ensure that sufficiently many nearest-neighbour candidates are found.

3 Cell Resampling for the Production of a W Boson with two Jets

We now demonstrate the proposed method through a highly non-trivial application. We consider the production of a leptonically decaying W^- boson together with at least two jets in proton-proton collisions at 14 TeV centre-of-mass energy calculated at next-to-leading

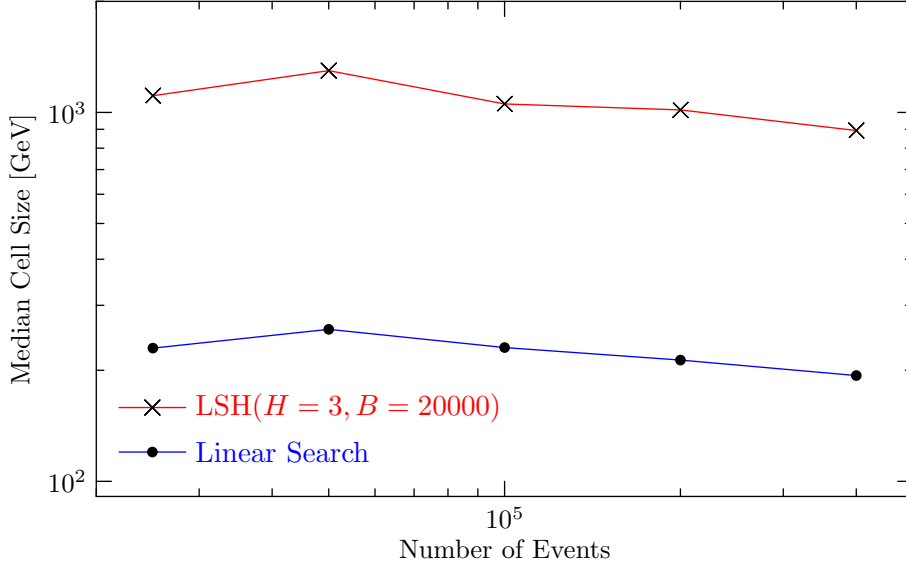


Figure 4: Comparison of the median cell size between linear nearest-neighbour search and the LSH-based approach with three hash functions.

order. Weighted events are generated using Sherpa [15] with OpenLoops [31]. Generation parameters are shown in table 1.

# events	6.1×10^7
μ_r, μ_f	$\frac{H_T}{2}$
\sqrt{s}	14 TeV
PDF	CT14nlo [32, 33]
Jet definition	anti- k_t [34], $R = 0.4$, $p_\perp > 30$ GeV
m_W	80.385 GeV
Γ_W	2.085 GeV
G_F	$1.1663787 \times 10^{-5} \text{ GeV}^{-2}$

Table 1: Parameters used for event generation.

The 2-parton samples receive contributions from Born, virtual, and subtraction terms, and the 3-parton samples from subtraction and real emission. The sum should be positive, provided reasonable choices for the renormalisation and factorisation scales have been applied. We choose $\mu_f = \mu_r = H_T/2$. The subtraction terms can extend far in phase space, which can cause non-local bin-to-bin migration in an analysis of distributions, and issues for the current resampling based on phase space buckets. This issue can be reduced by applying the modified subtractions [35, 36] to restrict their size. We have not done so in the current study, partly to illustrate the performance of the resampler in a “worst case” scenario. The results of the NLO calculation would obviously have less statistical jitter with a larger event sample — however, the purpose of this study is not to showcase the best possible results from NLO, but to illustrate how stable results can be obtained with

from a less-stable statistical sample, in this case from a NLO calculation.

For the cell resampling, we choose the distance measure introduced in section 2.1.1, and determine the contribution from transverse momentum differences by setting the parameter τ to 10, c.f. equation (2.10). Since the computing time required for cell resampling grows quadratically with the number of events, we split the original sample into nine samples of equal size and apply the resampling separately to each of them. At the same time, we impose an upper limit for the cell radius of 100 in order to achieve cell sizes commensurate with the combined sample size. While this limit prevents us from eliminating *all* negative event weights, it still reduces their overall contribution by more than an order of magnitude. This is illustrated in figure 5.

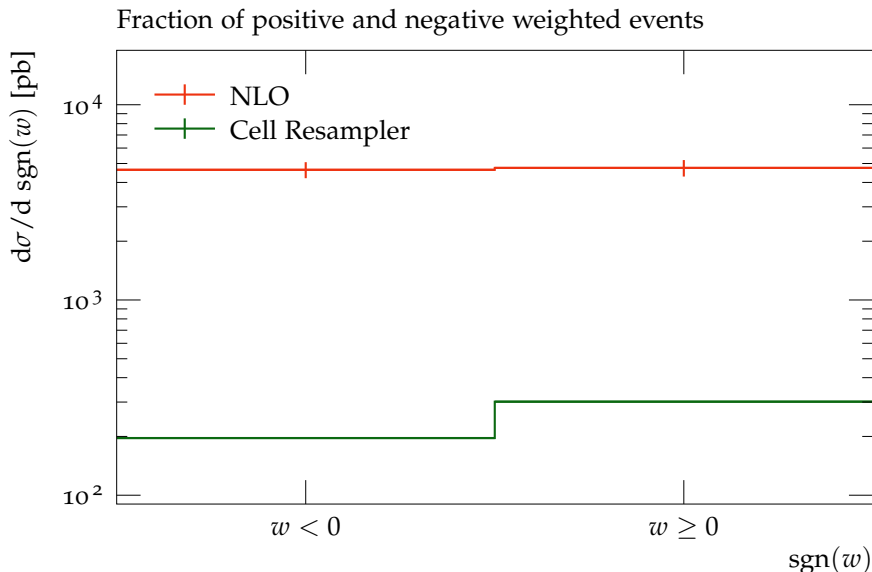


Figure 5: Contributions of negative- and positive-weight events to the cross section according to the MC_XS RIVET analysis.

The NLO calculation achieves a $\sim 10^2$ pb cross section as cancellation between terms of size $\sim 5 \times 10^3$ pb, whereas the cell resampler obtains the same cross section as a difference between terms of $\sim 3 \times 10^2$ pb and $\sim 2 \times 10^2$ pb. If we were to reweight the events to weight ± 1 , the original NLO sample would result in almost 20 times as many events compared to unweighting the resampled events. This corresponds to a Monte Carlo estimate of the uncertainty which is larger by a factor of approximately $\sim \sqrt{20}$. Conversely, to achieve the same estimated uncertainty as reached after resampling, a pure NLO sample would require the generation of almost 20 times as many events.

The events are parsed through the standard RIVET [37] analyses MC_WINC and MC_WJETS, plus a relevant ATLAS analysis [38] in to demonstrate the performance for calculations relevant for experimental measurements. As the point of this study is not to compare with experimental data, but to improve on the stability of the predictions, we will for simplicity use the calculation of just $pp \rightarrow e^- \bar{\nu}_e jj$ and not the positron channel.

Figure 6 compares the vanilla prediction for the NLO calculation and the result of

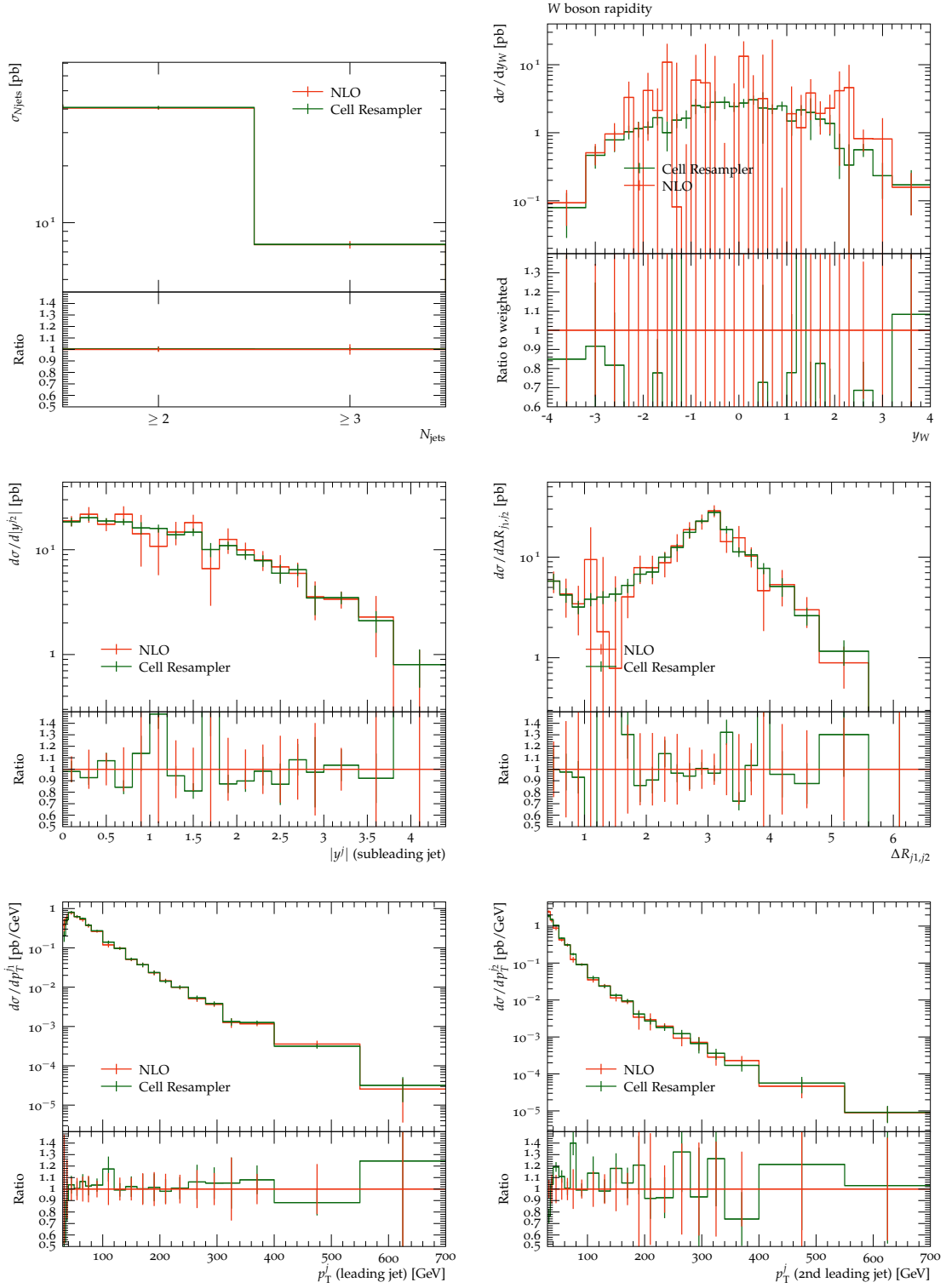


Figure 6: The results from the pure NLO calculation and of resampler for a subset of the analyses performed. See text for further details.

passing the NLO events through the resampler for several observables. The results for the inclusive two and three jet cross sections are shown in the top left plot. Both the NLO result and that of the cell resampler are stable, as expected. The vertical lines indicate the statistical uncertainty estimated from the weight distribution interpreted as a Monte Carlo sample. As such, the correlation between the weights of the counter events in Born and real emission phase space is not taken into account in this estimate. The estimate of the uncertainty is larger from the pure NLO sample than that of the cell resampler, simply because of the reduction in the variance of the weights in the event sample.

It would of course be unsatisfactory if the estimate of the Monte Carlo uncertainty was reduced without a stabilisation of predicted distributions. However, the results on the top right plot of the rapidity-distribution of the W boson (from the Rivet analysis `MC_WINC`) clearly show that the output of the cell resampler is significantly smoother than that of the vanilla NLO calculation, and that for both results the Monte Carlo estimate of the uncertainty in each bin correlates well with the statistical jitter between bins. Therefore we conclude that the reduction in the Monte Carlo estimate of the uncertainty of the inclusive rates in the previous plot is a reflection of smoother distributions. It is important to note here that contrary to the approach in [20], there is no input to the cell resampler about any analyses intended for the sample. This implies that the improvements seen would not be limited to the rapidity distribution of the W boson. Indeed, the plots on the middle row of figure 6 show that improvements are also seen in the distribution in the absolute rapidity of the hardest jet, $|y_{j_1}|$ and $\Delta R_{j_1, j_2}$, all calculated according to the analysis in [38].

Finally, the bottom row in figure 6 shows the distributions on the transverse momentum of the hardest and second hardest jet. These distributions are significantly smoother straight from the NLO calculation. They are smoother still from the cell resampler.

4 Conclusions

We have presented *cell resampling* as a method to eliminate negative event weights. Negative weights are redistributed *locally* in phase space and any potential bias introduced by this redistribution becomes arbitrarily small given sufficient statistics.

We have demonstrated the real-world performance on the highly non-trivial example of the production of a W boson with two jets at NLO. It is straightforward to apply our method to arbitrary processes, and we provide an easy-to-use implementation available from <https://cres.hepforge.org/> to this end.

A central ingredient of cell resampling is the definition of a *distance function* between events in phase space. This function should mirror experimental sensitivity without referring to any specific analysis. We have proposed a simple metric, which is shown to perform well in practice. The exploration of more sophisticated distance functions is a promising avenue towards future improvements of the cell resampling method.

Since the quality of the reweighted event samples increases systematically with their size, it is important that the computational cost of cell resampling scales well with the number of input events. To achieve this, we have explored an algorithm for nearest-

neighbour search in phase space based on random projections and locality-sensitive hashing. While we find a significantly improved scaling behaviour compared to naive linear search, further improvements will be necessary to obtain the same increase in quality with growing statistics.

Acknowledgements

This work has received funding from the European Union’s Horizon 2020 research and innovation programme as part of the Marie Skłodowska-Curie Innovative Training Network MCnetITN3 (grant agreement no. 722104), and the EU TMR network SAGEX agreement No. 764850 (Marie Skłodowska-Curie).

References

- [1] S. Catani and M. H. Seymour, *A General algorithm for calculating jet cross-sections in NLO QCD*, *Nucl. Phys. B* **485** (1997) 291–419, [[hep-ph/9605323](#)].
- [2] S. Catani, S. Dittmaier, M. H. Seymour and Z. Trocsanyi, *The Dipole formalism for next-to-leading order QCD calculations with massive partons*, *Nucl. Phys. B* **627** (2002) 189–265, [[hep-ph/0201036](#)].
- [3] S. Frixione and B. R. Webber, *Matching NLO QCD computations and parton shower simulations*, *JHEP* **06** (2002) 029, [[hep-ph/0204244](#)].
- [4] P. Nason and G. Ridolfi, *A Positive-weight next-to-leading-order Monte Carlo for Z pair hadroproduction*, *JHEP* **08** (2006) 077, [[hep-ph/0606275](#)].
- [5] J. C. Collins, D. E. Soper and G. F. Sterman, *Transverse Momentum Distribution in Drell-Yan Pair and W and Z Boson Production*, *Nucl. Phys. B* **250** (1985) 199–224.
- [6] V. S. Fadin, E. Kuraev and L. Lipatov, *On the Pommeranchuk Singularity in Asymptotically Free Theories*, *Phys. Lett. B* **60** (1975) 50–52.
- [7] I. I. Balitsky and L. N. Lipatov, *The Pommeranchuk singularity in quantum chromodynamics*, *Sov. J. Nucl. Phys.* **28** (1978) 822–829.
- [8] S. Höche, F. Krauss, M. Schönherr and F. Siegert, *QCD matrix elements + parton showers: The NLO case*, *JHEP* **04** (2013) 027, [[1207.5030](#)].
- [9] L. Lönnblad and S. Prestel, *Merging Multi-leg NLO Matrix Elements with Parton Showers*, *JHEP* **03** (2013) 166, [[1211.7278](#)].
- [10] L. Lönnblad and S. Prestel, *Unitarising Matrix Element + Parton Shower merging*, *JHEP* **02** (2013) 094, [[1211.4827](#)].
- [11] GEANT4 collaboration, S. Agostinelli et al., *GEANT4—a simulation toolkit*, *Nucl. Instrum. Meth. A* **506** (2003) 250–303.
- [12] J. Alwall, R. Frederix, S. Frixione, V. Hirschi, F. Maltoni, O. Mattelaer et al., *The automated computation of tree-level and next-to-leading order differential cross sections, and their matching to parton shower simulations*, *JHEP* **07** (2014) 079, [[1405.0301](#)].
- [13] J. Bellm et al., *Herwig 7.0/Herwig++ 3.0 release note*, *Eur. Phys. J. C* **76** (2016) 196, [[1512.01178](#)].

- [14] T. Sjöstrand, S. Ask, J. R. Christiansen, R. Corke, N. Desai, P. Ilten et al., *An Introduction to PYTHIA 8.2*, *Comput. Phys. Commun.* **191** (2015) 159–177, [[1410.3012](#)].
- [15] SHERPA collaboration, E. Bothmann et al., *Event Generation with Sherpa 2.2*, *SciPost Phys.* **7** (2019) 034, [[1905.09127](#)].
- [16] R. Frederix, S. Frixione, S. Prestel and P. Torrielli, *On the reduction of negative weights in MC@NLO-type matching procedures*, [2002.12716](#).
- [17] C. Gao, J. Isaacson and C. Krause, *i-flow: High-dimensional Integration and Sampling with Normalizing Flows*, *Mach. Learn. Sci. Tech.* **1** (2020) 045023, [[2001.05486](#)].
- [18] E. Bothmann, T. Janßen, M. Knobbe, T. Schmale and S. Schumann, *Exploring phase space with Neural Importance Sampling*, *SciPost Phys.* **8** (2020) 069, [[2001.05478](#)].
- [19] C. Gao, S. Höche, J. Isaacson, C. Krause and H. Schulz, *Event Generation with Normalizing Flows*, *Phys. Rev. D* **101** (2020) 076002, [[2001.10028](#)].
- [20] J. R. Andersen, C. Gütschow, A. Maier and S. Prestel, *A Positive Resampler for Monte Carlo events with negative weights*, *Eur. Phys. J. C* **80** (2020) 1007, [[2005.09375](#)].
- [21] B. Nachman and J. Thaler, *Neural resampler for Monte Carlo reweighting with preserved uncertainties*, *Phys. Rev. D* **102** (2020) 076004, [[2007.11586](#)].
- [22] B. Stienen and R. Verheyen, *Phase Space Sampling and Inference from Weighted Events with Autoregressive Flows*, [2011.13445](#).
- [23] P. T. Komiske, E. M. Metodiev and J. Thaler, *Metric Space of Collider Events*, *Phys. Rev. Lett.* **123** (2019) 041801, [[1902.02346](#)].
- [24] M. Crispim Romão, N. F. Castro, J. G. Milhano, R. Pedro and T. Vale, *Use of a generalized energy Mover’s distance in the search for rare phenomena at colliders*, *Eur. Phys. J. C* **81** (2021) 192, [[2004.09360](#)].
- [25] M. Cacciari and G. P. Salam, *Dispelling the N^3 myth for the k_t jet-finder*, *Phys. Lett. B* **641** (2006) 57–61, [[hep-ph/0512210](#)].
- [26] P. Indyk and R. Motwani, *Approximate nearest neighbors: Towards removing the curse of dimensionality*, in *Proceedings of the 30th ACM Symposium on Theory of Computing*, p. 604–613, 1998.
- [27] J. Leskovec, A. Rajaraman and J. Ullman, *Mining of Massive Datasets*. Cambridge University Press, 2020.
- [28] W. B. Johnson and J. Lindenstrauss, *Extensions of Lipschitz mappings into a Hilbert space*, *Contemp. Math.* (1984) 189–206.
- [29] M. E. Muller, *A Note on a Method for Generating Points Uniformly on N -Dimensional Spheres*, *Comm. Assoc. Comput. Mach.* **2** (1959) 19–20.
- [30] G. Marsaglia, *Choosing a Point from the Surface of a Sphere*, *Ann. Math. Stat.* **43** (1972) 645–646.
- [31] F. Buccioni, J.-N. Lang, J. M. Lindert, P. Maierhöfer, S. Pozzorini, H. Zhang et al., *OpenLoops 2*, *Eur. Phys. J. C* **79** (2019) 866, [[1907.13071](#)].
- [32] S. Dulat, T.-J. Hou, J. Gao, M. Guzzi, J. Huston, P. Nadolsky et al., *New parton distribution functions from a global analysis of quantum chromodynamics*, *Phys. Rev. D* **93** (2016) 033006, [[1506.07443](#)].

- [33] A. Buckley, J. Ferrando, S. Lloyd, K. Nordström, B. Page, M. Rüfenacht et al., *LHAPDF6: parton density access in the LHC precision era*, *Eur. Phys. J. C* **75** (2015) 132, [[1412.7420](#)].
- [34] M. Cacciari, G. P. Salam and G. Soyez, *The anti- k_t jet clustering algorithm*, *JHEP* **04** (2008) 063, [[0802.1189](#)].
- [35] Z. Nagy, *Three jet cross-sections in hadron hadron collisions at next-to-leading order*, *Phys. Rev. Lett.* **88** (2002) 122003, [[hep-ph/0110315](#)].
- [36] Z. Nagy, *Next-to-leading order calculation of three jet observables in hadron hadron collision*, *Phys. Rev. D* **68** (2003) 094002, [[hep-ph/0307268](#)].
- [37] C. Bierlich et al., *Robust Independent Validation of Experiment and Theory: Rivet version 3*, *SciPost Phys.* **8** (2020) 026, [[1912.05451](#)].
- [38] ATLAS collaboration, G. Aad et al., *Measurements of the W production cross sections in association with jets with the ATLAS detector*, *Eur. Phys. J. C* **75** (2015) 82, [[1409.8639](#)].